# Raman spectroscopy combined with comprehensive gas chromatography for label-free characterization of plasma-derived extracellular vesicle subpopulations

Liangsupree, Thanaporn

2022-06-15

Liangsupree , T , Multia , E , Saarinen , J , Ruiz-Jimenez , J , Kemell , M & Riekkola , M-L 2022 , ' Raman spectroscopy combined with comprehensive gas chromatography for label-free characterization of plasma-derived extracellular vesicle subpopulations ' , Analytical Biochemistry , vol. 647 , 114672 . https://doi.org/10.1016/j.ab.2022.114672

http://hdl.handle.net/10138/346837
https://doi.org/10.1016/j.ab.2022.114672

Analytical Biochemistry 647 (2022) 114672

Contents lists available at ScienceDirect

Analytical Biochemistry

journal homepage: www.elsevier.com/locate/yabio

# Raman spectroscopy combined with comprehensive gas chromatography for label-free characterization of plasma-derived extracellular vesicle subpopulations

Thanaporn Liangsupree [a], Evgen Multia [a], Jukka Saarinen [b], Jose Ruiz-Jimenez [a], Marianna Kemell [a], Marja-Liisa Riekkola [a,*]

[a] Department of Chemistry, P.O. Box 55, FI-00014, University of Helsinki, Finland
[b] Drug Research Program, Division of Pharmaceutical Chemistry and Technology, P.O. Box 56, FI-00014, University of Helsinki, Finland

ARTICLE INFO

*Keywords:*
Raman spectroscopy
Comprehensive two-dimensional gas chromatography
Extracellular vesicles
Exomeres
Exosomes
Isolates

ABSTRACT

Raman spectroscopy together with comprehensive two-dimensional gas chromatography–time-of-flight mass spectrometry (GCxGC–TOFMS) was employed to characterize exomere- (<50 nm) and exosome-sized (50–80 nm) EVs isolated from human plasma by the novel on-line immunoaffinity chromatography – asymmetric flow field-flow fractionation method. $CD9^+$, $CD63^+$, and $CD81^+$ EVs were selected to represent general EV subpopulations secreted into plasma, while $CD61^+$ EVs represented the specific EV subset derived from platelets. Raman spectroscopy could distinguish EVs from non-EV particles, including apolipoprotein B-100-containing lipoproteins, signifying its potential in EV purity assessment. Moreover, platelet-derived ($CD61^+$) EVs of both exomere and exosome sizes were discriminated from other EV subpopulations due to different biochemical compositions. Further investigations demonstrated composition differences between exomere- and exosome-sized EVs, confirming the applicability of Raman spectroscopy in distinguishing EVs, not only from different origins but also sizes. In addition, fatty acids that act as building blocks for lipids and membranes in EVs were studied by GCxGC—TOF-MS. The results achieved highlighted differences in EV fatty acid compositions in both esterified (membrane lipids) and non-esterified (free fatty acids) fractions, indicating possible differences in membrane structures, biological functions, and roles in cell-to-cell communications of EV subpopulations.

## 1. Introduction

Extracellular vesicles (EVs) are heterogeneous nanosized lipid vesicles (30–5000 nm in diameter) originated from various cells. EVs play essential roles in intercellular communication by carrying and transporting biological components to recipient cells [1]. Among EV subclasses, exosomes (50–150 nm) generated via the endosomal pathway, have gained increasing interest in recent years due to their potential in diagnostic and therapeutic applications, such as biomarker profiling, disease progression, and drug delivery [2]. The smaller EV subclass (under 50 nm), namely exomere, has been recently identified using asymmetric flow field-flow fractionation (AsFlFFF or AF4) [3–5]. Exomeres and exosomes derived from the same cell types have been shown to differ in cargoes and biophysical properties, suggesting that they could have different biogenesis and thus possibly different roles in cell-to-cell communication [3]. EVs of similar size ranges, including $CD9^+$ and platelet-derived or $CD61^+$, have been isolated and fractionated from human plasma using our recently developed on-line immunoaffinity chromatography – asymmetric flow field-flow fractionation method (IAC – AsFlFFF) [5]. Further analyses indicated that the isolated and fractionated EV subpopulations differed in amino acid and sugar compositions [5].

Despite the growing interest in EVs, studies of their subpopulations have been hindered by limitations of conventional isolation techniques, particularly when isolating EVs from complex biological matrices, such as blood plasma, as EVs tend to co-isolate with other particles sharing the same size as EVs (e.g., lipoproteins) [6]. Only a few techniques, such as AsFlFFF, can overcome the drawbacks of conventional techniques and thus enable further elucidation and compositional studies of distinct EV subpopulations. Moreover, various techniques routinely used for EV characterization and analysis, such as flow cytometry and Western blot, are often time-consuming, require expensive reagents, and only provide

* Corresponding author.
*E-mail address:* marja-liisa.riekkola@helsinki.fi (M.-L. Riekkola).

https://doi.org/10.1016/j.ab.2022.114672
Received 2 October 2021; Received in revised form 12 March 2022; Accepted 22 March 2022
Available online 5 April 2022

specific information on EV characteristics. On the other hand, recent studies have shown applications of Raman spectroscopy as an alternative tool for characterization, compositional studies, and purity assessment of EVs [7–10]. Raman spectroscopy, based on inelastic scattering of light, is beneficial in being a label-free, chemical-specific, and relatively non-destructive technique detecting molecular vibrations that can identify essential components present in EVs, such as membrane lipids, proteins, and nucleic acids [11]. Consequently, it holds potential as a quick and simple technique to comparatively study compositions and evaluate the purity of EV subpopulations having different sizes, e.g., exomere- and exosome-sized EVs, and origins, such as EVs released from platelets ($CD61^+$ EVs) and other EVs found in the circulation.

In this study, $CD9^+$, $CD63^+$, $CD81^+$ (selected to represent "universal" EV subsets secreted from all cells into plasma) and $CD61^+$ (for platelet-derived EVs) EV subpopulations of <50 nm exomere-sized and 50–80 nm exosome-sized were isolated from human plasma using our recently developed IAC – AsFlFFF system [5]. Raman spectroscopy together with comprehensive two-dimensional gas chromatography – time-of-flight mass spectrometry (GCxGC—TOFMS) was used to elucidate biochemical compositions of the EV subpopulations. EV purity was assessed by comparing their Raman spectra to pre-isolated apolipoprotein B-100 (apoB-100)-containing lipoproteins which are known to co-isolate with EVs acquired using conventional techniques. Multivariate approach of principal component analysis (PCA) was used to statistically determine spectral similarities and differences among the samples, while linear discriminant analysis (LDA) and support vector machine (SVM) were performed to confirm the differences found in the samples. To gain extra insight into lipid compositions, GCxGC—TOFMS was employed to elucidate fatty acid (esterified and non-esterified) compositions of EVs, apoB-100-containing lipoproteins, and plasma. To the extent of our knowledge, this is the first study that investigates and characterizes highly specific EV subpopulations of different sizes from human plasma using Raman spectroscopy combined with GCxGC—TOFMS, especially those of exomere-sized subpopulations which have been scarcely studied, since they have only been recently discovered.

## 2. Materials and methods

### 2.1. Chemicals and materials

Phosphate buffered saline (PBS) tablets, HCl (fuming 37%), and ethanolamine were purchased from Sigma-Aldrich (St. Louis, MO, USA). $NaHCO_3$ and $Na_2CO_3$ were purchased from Merck KGaA (Darmstadt, Germany). MilliQ water was obtained using the MilliQ system (Millipore, USA). Methanol (purity ≥99.9%), dichloromethane (DCM) (purity ≥99.8%), and n-hexane (purity ≥97.0%) were purchased from Riedel-de Haën (Seelze, Germany). KOH was purchased from Fisher Scientific. Sulphuric acid (95%) was purchased from VWR Chemicals. Sodium sulfate anhydrous was obtained from Fluka Chemika. Human plasma samples were obtained from Finnish Red Cross Blood Service with permission number 30/2020. Low-density lipoprotein (LDL) samples were isolated from human plasma using ultracentrifugation as described in Ref. [12] and provided by Dr. Katariina Öörni from Wihuri Research Institute. Anti-human-apolipoprotein B-100 monoclonal antibody (anti-apoB-100 mAb) (Medix Biochemica Co. Inc., Helsinki, Finland) was provided by Dr. Matti Jauhiainen from Minerva Foundation Institute for Medical Research. Purified mouse anti-human CD61 clone VI-PL2 (anti-CD61), anti-human CD63 clone H5C6 (anti-CD63), and anti-human CD81 clone JS-81 (anti-CD81) antibodies were purchased from BD Biosciences (USA), while anti-CD9 monoclonal antibody was purchased from ThermoFisher (Rockford, IL, USA). Micro BCA Protein Assay Kit (catalog number 23235) was purchased from Pierce/-ThermoFisher (Rockford, IL, USA). Alkane standard solutions $C_8$–$C_{20}$ and $C_{21}$–$C_{40}$, methyl heptadecanoate-$d_{33}$ (purity ≥97.5%), and certified reference material (CRM47885) containing 37 fatty acid methyl ester (FAME) standards (Supelco® 37 Component FAME Mix) were purchased from Sigma Aldrich (PA, USA).

### 2.2. Instrumentation

Convective Interaction Media® (CIM®) carbonyldiiimidazole (CDI) monolithic chromatographic columns and housing cartridges were purchased from BIA Separations (Ljubljana, Slovenia). All instrumentation for the AsFlFFF system was described in our previous study [5]. Supor®-200 membrane filters (0.2 μm) (PALL Life Sciences, USA) were used to filter the PBS buffer. Low Protein Binding Hydrophilic LCR (PTFE) membrane filters (0.45 μm) (Millipore, USA) were used to filter plasma samples. Nanosep centrifugal devices with a 10 K molecular weight cut-off (MWCO) membrane filters (Pall Corporation, New York, USA) were used to pre-concentrate EV fractions prior to Raman spectroscopy measurements and field-emission scanning electron microscopy (FESEM) imaging. Absorbance for total protein concentrations in all samples was measured using EnSpire Multimode Plate Reader (PerkinElmer Inc., USA). SEM images were taken with a Hitachi S-4800 FESEM (Hitachi, Japan). A confocal Raman microscope (NT-MDT Ntegra, Russia) equipped with a 532 nm continuous wave laser (output power ~ 20 mW) and a 100 × objective (Mitutoyo, Japan) was used to acquire Raman spectra. Analysis of fatty acid methyl esters (FAMEs) was done with a LECO Pegasus 4D comprehensive two-dimensional gas chromatography (GCxGC) – time-of-flight mass spectrometer (TOFMS). The gas chromatography system consisted of an autosampler (7683B) and a gas chromatograph (7890A) (Agilent Technologies, Santa Clara, CA, USA). Retention gap (deactivated fused silica) (2.5 m × 0.25 mm i.d.) and first dimension column (HP-5MS Ultra Inert, 30 m × 0.25 mm i.d., 0.25 μm film thickness) were purchased from Agilent Technologies (Santa Clara, CA, USA). The second dimension column was an ionic liquid column with intermediate polarity (SLB-IL82, 1.5 m × 0.10 mm i.d., 0.08 μm film thickness) purchased from Supelco Sigma Aldrich (PA, USA).

### 2.3. Isolation and fractionation of extracellular vesicles and apolipoprotein B-100-containing lipoproteins

Isolation and fractionation of EVs and apoB-100 containing lipoproteins were done by on-line IAC-AsFlFFF described in our previous study [5,13]. IAC in this study included five separate monolithic disks immobilized with different ligands. For the EV isolation, four different monolithic disks immobilized with anti-CD9, anti-CD63, anti-CD81, and anti-CD61 (0.5 mg/mL, 1 mL) were prepared according to our previous protocol [4,13] and used to isolate $CD9^+$, $CD63^+$, $CD81^+$, and $CD61^+$ EVs, respectively. The anti-apoB-100 mAb having affinity toward apoB-100-containing lipoproteins (i.e. very-low-density lipoproteins (VLDL), intermediate-density lipoproteins (IDL), and low-density lipoproteins (LDL) [14–16]) was immobilized on the monolithic disk as previously described [12]. The anti-apoB-100 disk was subsequently used for the isolation of the mixture of apoB-100-containing lipoproteins. Human plasma samples were 1:10 (v:v) diluted in PBS, pH 7.4 (500 mL of plasma in 4.5 mL of PBS), and filtered with 0.45 μm syringe filters prior to injection to IAC-AsFlFFF system. Fractionated EV subpopulations and apoB-100-containing lipoproteins were collected for further analysis.

### 2.4. Total protein analysis

Total protein concentrations in plasma, apoB-100-containing lipoproteins, and EV samples were measured using bicinchoninic acid (BCA) assay [17] with Micro BCA Protein Assay Kit according to the manufacturer's protocol. The absorbance was measured at 562 nm using EnSpire Multimode Plate Reader (PerkinElmer Inc., USA). Protein concentrations were calculated using EnSpire Workstation software (version 4.13.3005.1482).

### 2.5. Imaging of EV subpopulations using scanning electron microscopy (SEM)

EV imaging using SEM was done as previously described in Ref. [5]. Briefly, EVs were concentrated using disposable Nanosep centrifugal devices with 10 K MWCO membrane filters. The pre-concentrated EVs were air-dried on silicon wafer surfaces, coated with a 3 nm Au–Pd alloy, and imaged with secondary electrons (3 kV).

### 2.6. Characterization of extracellular vesicle subpopulations by Raman spectroscopy

#### 2.6.1. Sample preparation and Raman spectroscopy experiments

The isolated and fractionated EVs and apoB-100-containing lipoproteins were pre-concentrated using disposable Nanosep centrifugal devices with 10 K MWCO membrane filters. Human plasma, LDL isolated using ultracentrifugation, and the pre-concentrated EV subpopulations and apoB-100-containing lipoproteins isolated using the IAC-AsFlFFF system (2 μL) were deposited on a $CaF_2$ substrate (Laser-Optex Inc., China) and air-dried. The samples were analyzed using a confocal Raman microscope equipped with a 532 nm continuous wave laser and a 100 × objective. Measurements were done using a back-scattering geometry. Prior to the analysis, a silicon Raman peak at 520.7 $cm^{-1}$ was used to calibrate the system. Spectral resolution with 1800/500 grating was ~4.4 $cm^{-1}$ (obtained by measuring the full width at half maximum (FWHM) of silicon Raman peak at 520.7 $cm^{-1}$). The spectra were collected in the spectral range of 750-1900 $cm^{-1}$ (fingerprint region) and 2800-3200 $cm^{-1}$ (C–H stretching region). The measurement was done 10 times for each sample, and an exposure time of 10 s with an accumulation of 2 was used for the acquisition of a single spectrum. Raman spectra were measured on the edge of the dried sample (Fig. S1).

#### 2.6.2. Data processing and analysis

Raw Raman spectra in the fingerprint region (750-1900 $cm^{-1}$) and C–H stretching region (2800-3200 $cm^{-1}$) were baseline-subtracted using the anchor point finding method (second derivatives (zeros), 8 points) in OriginPro (9.7.0.188). Thereafter, the baseline-subtracted spectra were normalized using the standard normal variate (SNV) approach [18]. This study utilized different R 3.6.3 statistical analysis tools for data analysis. The baseline-subtracted and normalized data were further analyzed using the multivariate approach of principal component analysis (PCA), linear discriminant analysis (LDA) [19], and support vector machine (SVM) [20]. PCA was firstly performed on the spectra obtained from EV samples (n = 80) and non-EV samples (plasma and lipoproteins) (n = 30) to visualize possible differences between the non-EV and EV samples. Further PCAs were done to visualize the differences between spectra obtained from exomere- and exosome-sized (n = 40 each) as well as $CD9^+$, $CD63^+$, $CD81^+$, and $CD61^+$ (n = 20 each) EV subpopulations. In order to statistically confirm classification accuracy, LDA and SVM were additionally performed. Since SVM algorithm is more suitable for a relatively large number of samples, it was utilized for classification of EV and non-EV components. On the other hand, LDA provides higher prediction capability for a relatively small sample size, and thus it was applied for classification among EV subpopulations.

### 2.7. Studies of fatty acids in EV subpopulations by comprehensive two-dimensional gas chromatography – time-of-flight mass spectrometry

#### 2.7.1. Sample preparation

Fatty acids in plasma, apoB-100-containing lipoproteins, and EVs analyzed with Raman spectroscopy were further identified and quantified using GCxGC—TOFMS. Firstly, methylation of fatty acids in EVs was performed according to the previously reported protocol [21] with slight modifications. Briefly, 400 μL of each EV and apoB-100-containing lipoprotein fraction was concentrated under $N_2$ to the final volume of 50 μL, while for plasma, the starting volume was 50 μL. Each sample was added with KOH–$CH_3OH$ (0.5 mL, 0.4 M) and left to stand at room temperature for 10 min. Thereafter, n-hexane (0.5 mL) was added twice to the mixture and vortexed for 30 s each. The hexane phase containing esterified fatty acid methyl esters was collected, dried under $N_2$, and reconstituted with 50 μL of DCM and 5 μL ISTD (methyl heptadecanoate-$d_{33}$). In order to obtain non-esterified fatty acid methyl esters, the residue phase was added with anhydrous sodium sulfate to remove water then with $H_2SO_4$–$CH_3OH$ (0.5 mL, 1 M), vortexed, and ultrasonicated at room temperature for 20 min. Then, the mixture was added with n-hexane (0.5 mL) twice and vortexed for 30 s each. The hexane phase was acquired and dried under $N_2$ and reconstituted with DCM and ISTD as described earlier. The prepared samples were then studied by comprehensive GCxGC—TOFMS. PBS was used as a blank.

#### 2.7.2. Studies of fatty acids by GCxGC – TOFMS

Esterified and non-esterified fatty acid methyl esters in EV subpopulations were studied by GCxGC—TOFMS. The GCxGC method was adopted from Ref. [22] with modifications. The chromatographic separation by GCxGC was performed using a splitless injection mode (1 μL) with an injector temperature of 250 °C. The primary oven temperature program was set at 40 °C for 3 min, followed by a temperature increase to 160 °C (10 °C/min), and finally to 250 °C (2 °C/min) for 10 min. The secondary oven temperature was 5 °C higher than the primary oven with a final temperature of 255 °C. Helium was used as a carrier gas. The modulation period was 4 s. The transfer line temperature was maintained at 255 °C. The TOFMS utilized the electron impact ionization at 70 eV at 220 °C. The detector voltage was 1850 V, and the data within the mass range of *m/z* 50-650 was collected (50 spectra per second) with an acquisition delay of 8 min. FAME standards and esterified and non-esterified fatty acids from plasma, apoB-100-containing lipoproteins, and EV samples were analyzed in triplicate.

#### 2.7.3. Data handling and analysis

Chromatographic data were processed using LECO ChromaTOF software (Version 4.72.0.0 optimized for Pegasus) using retention indices generated with analyzed alkane series. Identification of FAMEs in standards was done by manually comparing their retention indices and mass spectra with NIST 14 MS database and MS Search Version 2.2. Compounds having hit similarity less than 700 were excluded as described in Ref. [23]. The identification of FAMEs in human plasma, apoB-100-containing lipoproteins, and EV samples was performed by comparing the retention time and mass spectra to the FAME standards. Extracted ion chromatograms (EICs) obtained using representative mass-to-charge (*m/z*) ratios (Table S1) were used for quantification of the detected FAMEs. Calibration curves were obtained using relative peak areas of the EICs. Data of the samples were subtracted with PBS response. Finally, relative peak areas of each sample were dilution corrected and normalized using their corresponding total protein contents measured with the micro protein BCA assay.

## 3. Results and discussion

In this section, first, isolation and fractionation of EV subpopulations, including $CD9^+$, $CD63^+$, $CD81^+$, and $CD61^+$ EVs of exomere- (under 50 nm) and exosome-sized (50–80 nm) isolated and fractionated by our previously developed automated on-line IAC-AsFlFFF system [5] will be discussed. To further elucidate their biochemical profiles, the EV subpopulations along with plasma and lipoproteins were characterized using Raman spectroscopy. Multivariate approach of PCA was applied to assess the ability of Raman spectroscopy in differentiating EV subpopulations, while SVM and LDA were additionally performed to statistically confirm the differences and to determine the classification accuracy. To gain more in-depth insights into EV lipid compositions, esterified and non-esterified fatty acids present in the samples were identified and quantified using GCxGC—TOFMS.

### 3.1. Isolation and fractionation of apoB-100-containing lipoproteins and EV subpopulations from human plasma by on-line IAC-AsFlFFF

In this study, our previously developed on-line IAC-AsFlFFF system [5,13] was used to isolate and fractionate EV subpopulations and anti-apoB-100-containing lipoproteins from human plasma. In order to specifically isolate EV subpopulations, immunoaffinity chromatography was employed by utilizing four separate monolithic disks immobilized with monoclonal anti-tetraspanin (anti-CD9, anti-CD63, and anti-CD81) and anti-integrin (anti-CD61) antibodies. Anti-CD9, anti-CD63, and anti-CD81 disks targeted tetraspanin membrane proteins expressed on EVs from diverse cell types [24] and consequently yielding $CD9^+$, $CD63^+$, and $CD81^+$ EV subpopulations that represented general populations of EVs. On the other hand, the monolithic disk immobilized with anti-CD61 antibody was used to selectively isolate EVs derived from platelets as previously discussed in Ref. [4]. As shown in Fig. 1A, fractionation of EV isolates from all monolithic disks by AsFlFFF resulted in EVs with hydrodynamic diameters ranging from 20 to 90 nm as determined by the dynamic light scattering (DLS) detector. The EV subpopulations were subsequently divided into two size ranges: under 50 nm (exomere-sized EVs) and 50–80 nm (exosome-sized EVs) similar to the division done in our previous study [5]. FESEM images shown in Fig. 1B further confirmed intact EVs with preserved EV-shaped morphology. The corresponding EV sizes determined by FESEM were in good agreement with size ranges measured by DLS. Interestingly, the DLS (Fig. 1A) and UV fractograms (Figs. S2A–D) illustrated that the $CD63^+$ and $CD81^+$ isolates were more enriched in exomere-sized EVs compared to the fractionated isolates of $CD9^+$ and $CD61^+$ EVs. On the other hand, exosome-sized EVs were present in a relatively small amount regardless of immunoaffinity ligands used. Previous studies have also shown that expression profiles of tetraspanins in EVs of different sizes can vary [3,25,26] and depend on various factors, such as cell types or biological fluids from which EVs were isolated [27]. The eluting peak at 14–18 min in the UV fractograms (Fig. S2) were most likely disintegrated EV particles, as no DLS signals were detected and no accumulation of particles were observed at the edge of the dried droplet on the $CaF_2$ substrate under the bright-field confocal miscroscope (Fig. S2B).

In addition to EVs, on-line IAC-AsFlFFF was used to isolate apoB-100-containing lipoproteins using the anti-apoB-100 disk, and the isolate was fractionated, resulting in particles in the size ranges corresponding to VLDL (30–80 nm), IDL (23–27 nm), and LDL (18–25 nm) [28–30] based on DLS measurements (Fig. S2E). Consistent with our previous study [5], the isoabsorbance plots used for quality check of the fractionated isolates obtained from the diode array detector (DAD) contained the absorption band between 400 and 500 nm due to the presence of carotenoids, nutrient pigments commonly found in plasma and transported majorly by LDL [31], in the apoB-100-containing lipoprotein particles. In contrast, the carotenoid absorption was absent from all fractionated EVs, suggesting that the fractionated EV isolates did not contain a detectable amount of apoB-100-containing lipoprotein particles. Further characterization of LDL isolated using the anti-apoB-100 disk can be found in our previous study [12].

### 3.2. Characterization of plasma, apoB-100-containing lipoproteins, and EV subpopulations by Raman spectroscopy

#### 3.2.1. Human plasma and apoB-100-containing lipoproteins

Raman spectroscopy was used to assess purity and evaluate biochemical compositions of the EV subpopulations. Since lipoproteins, particularly apoB-100-containing lipoproteins, are present in relatively high concentrations in plasma and tend to co-isolate with EVs from

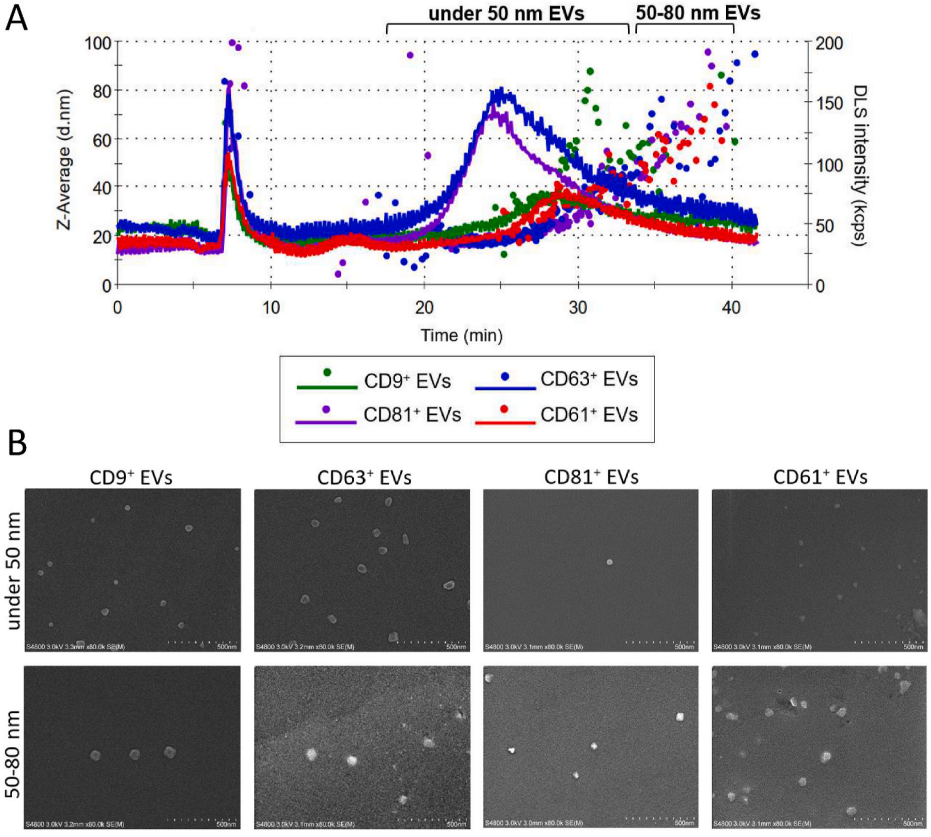


**Fig. 1.** Analysis profiles of isolated $CD9^+$, $CD63^+$, $CD81^+$, and $CD61^+$ EV subpopulations: A) AsFlFFF fractograms of isolated EVs showing hydrodynamic diameter (dotted) (Z-average, nm) and DLS intensity (line) (kcps), B) FESEM images showing size ranges and morphology of $CD9^+$, $CD63^+$, $CD81^+$, and $CD61^+$ EV subpopulations (Scale bar, 500 nm).

conventional isolation methods [6], it was essential to evaluate our newly developed IAC-AsFlFFF method for lipoprotein contaminants in the $CD9^+$, $CD63^+$, $CD81^+$, and $CD61^+$ EVs in both exomere and exosome size ranges. For this purpose, Raman spectra of LDL, isolated using the conventional ultracentrifugation (UC), and a mixture of apoB-100-containing lipoproteins, isolated using the IAC-AsFlFFF system, were acquired and used as references. Raman spectra (baseline-subtracted and normalized using the standard normal variate (SNV) method) in the fingerprint region (740-1870 $cm^{-1}$) (Fig. 2A) and the C–H stretching regions (2800-3200 $cm^{-1}$) (Fig. S3) showed characteristic features for major plasma compositions, including proteins and lipids similar to those for LDL and apoB-100-containing lipoproteins. Peak assignments were done based on previous studies [32–49] and summarized in Table S2. The presence of carotenoids was prominent in plasma, LDL, and apoB-100-containing lipoproteins at 1000-20, 1150-55, and 1514-38 $cm^{-1}$. This was in good agreement with the control isoabsorbance plots discussed earlier. In order to further distinguish the analyzed samples, PCA was performed for each recorded Raman spectrum in the fingerprint region (Fig. 2A), resulting in the scatter plot (Fig. 2B) and the loading plot (Fig. S4). PC-1 and PC-2 exhibiting the highest discriminative power were selected to distinguish the samples. The obtained PCA scatter plot (Fig. 2B) showed that scores from both UC-isolated LDL and apoB-100-containing lipoproteins were in the same region as plasma, separated from EV samples, indicating their similarities in biochemical compositions. In addition, LDL and apoB-100-containing lipoproteins could be partially separated from each other. Their differences were majorly due to carotenoids (1150 and 1521 $cm^{-1}$), and protein and lipid compositions (950-1050 and 1350-1400 $cm^{-1}$) as shown in the loading plot and spectral difference (Fig. S5). These differences were most likely caused by VLDL and IDL, present in the apoB-100-containing lipoprotein mixture in addition to LDL, while the UC-isolated LDL contained only pure LDL. The SVM result suggested that over 87% of the samples were accurately classified.

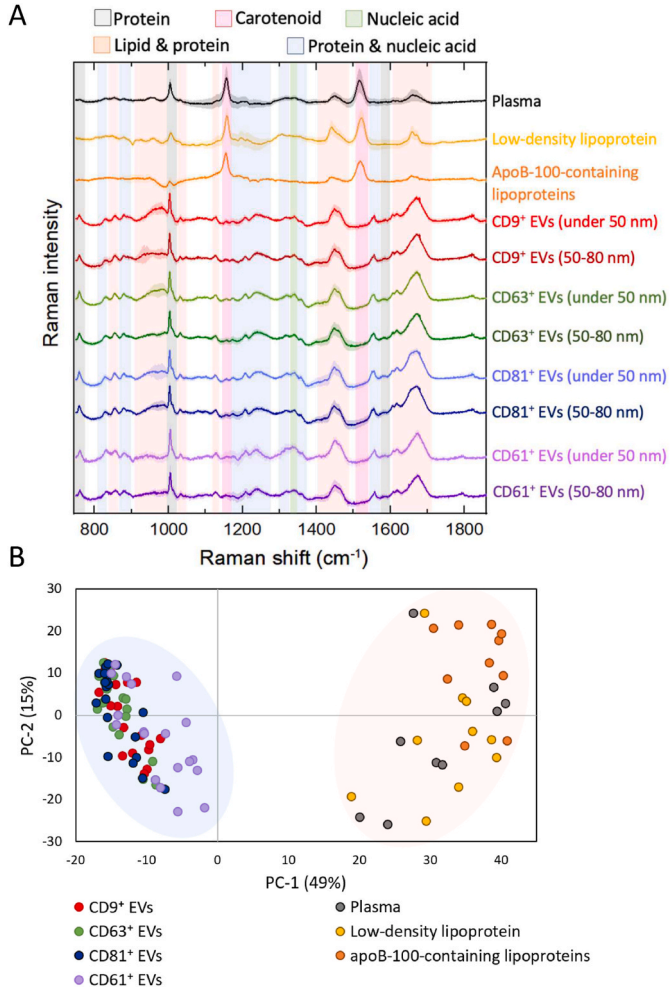


**Fig. 2.** Analysis of Raman spectra. (A) Average baseline-subtracted and standard normal variate (SNV)-normalized Raman spectra obtained from plasma, low-density lipoprotein (LDL) isolated by ultracentrifugation, apoB-100-containing lipoproteins isolated by the IAC-AsFlFFF, and EV subpopulations in the fingerprint region. Their corresponding standard deviations are displayed in the shaded area, and spectral ranges of biomolecular contributions are highlighted. (B) Scatter plot based on principal component analysis of each measured spectrum (outliers removed). EV subpopulations were categorized based on immunoaffinity ligands used during the isolation process.

### 3.2.2. *EV subpopulations*

Raman spectra of all EV samples (Fig. 2A) in the fingerprint region showed characteristic bands corresponding to major EV components, including proteins at 820-70 $cm^{-1}$ (proline (Pro) and hydroxyproline (Hyp)), 918-80 $cm^{-1}$ (Pro, valine (Val)), 1003 $cm^{-1}$ (phenylalanine (Phe)), 1127 $cm^{-1}$ (Pro), 1200-1350 $cm^{-1}$ (amide III), and 1656-80 $cm^{-1}$ (amide I), lipids at 877, 960-80, 1420-50, and 1652-70 $cm^{-1}$ as well as nucleic acids at 1288 $cm^{-1}$. The spectra from C–H stretching region (Fig. S3) also showed features corresponding to lipids and proteins at 2877 and 2936 $cm^{-1}$. In comparison to plasma and the apoB-100-containing lipoprotein spectra, the score clusters (Fig. 2B) of EVs could be clearly distinguished from the non-EV samples, suggesting their compositional differences. The loading plot (Fig. S4) further indicated that the major differences between EVs and other plasma components were due to carotenoids as also seen in Fig. 2A in which the carotenoid bands were absent at 1150 and 1521 $cm^{-1}$. This could be explained by the lack of carotenoids in EVs, indicating that the EVs isolated using the IAC-AsFlFFF system contained little to no apoB-100-containing lipoprotein contaminants, confirming their purity in regard to lipoprotein contaminations. These findings demonstrated that Raman spectroscopy can serve as a tool for both evaluations of lipoprotein contaminants in fractionated EV isolates and identification of different classes of large biomolecules found in the circulation.

*3.2.2.1. Exomere- and exosome-sized EVs.* In addition to the EV purity assessment, an important goal of this study was to elucidate biochemical compositions of the EV subpopulations. To further investigate the ability of the Raman spectroscopy to discriminate EVs of different sizes and origins, their subpopulations were first categorized into two groups based on the two different sizes and separately evaluated. PCA of Raman spectra obtained from exomere- and exosome-sized EVs in the fingerprint region resulted in the score plots (Figs. 3A and 4A) displaying scores assigned to each measured EV spectrum. Loadings of the PCs with the highest discriminative power between the sample sets (Figs. 3B and 4B) were used to identify spectral ranges that contributed to variations among the samples. The first analysis was made with the exomere-sized EVs in which the PC scores could be graphically classified into four clusters based on the ligands used for EV isolation seen in Fig. 3A. The PCA score plot showed overlapping clusters of $CD9^+$, $CD63^+$, and $CD81^+$ EVs, suggesting their spectral similarities and thus similar compositions in comparison with $CD61^+$ or platelet-derived EVs. In contrast, the $CD61^+$ EVs could be clearly distinguished from other EVs with PC-1 scores being the main contributor to their differences. The PC-1 loading plot (Fig. 3B) further indicated that the variations among exomere-sized EVs were due to spectra ranges at 924-1003 $cm^{-1}$ (proteins and lipids) and 1274-1571 $cm^{-1}$ (protein, lipids, and nucleic acids). It is important to note that even though the spectral range of 950–1000 $cm^{-1}$ can also be due to the inorganic salts present in the PBS [50], all EVs investigated in this study were resuspended with the same volume and concentration of PBS. Therefore, the differences found between EVs were due to lipid and protein composition rather than from

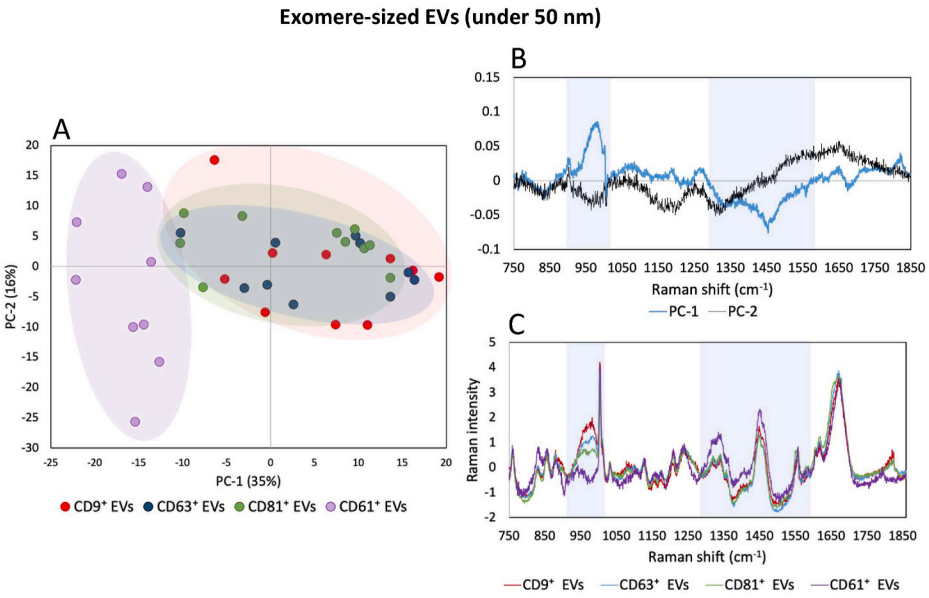


**Fig. 3.** Principal component analysis of baseline-subtracted and SNV-normalized Raman spectra of exomere-sized EVs (under 50 nm) including the score plot from the PCA (outliers removed) (A), PC-loading plot based on Raman shift (B), and average Raman spectra (C). PC-loading and spectrum intervals contributing to EV differences are highlighted.

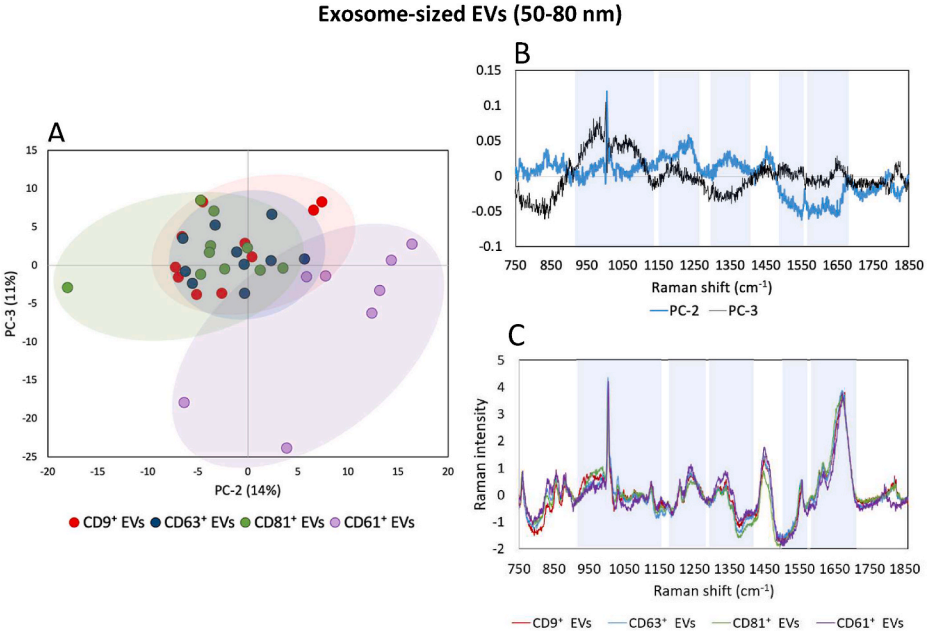


**Fig. 4.** Principal component analysis of baseline-subtracted and SNV-normalized Raman spectra of exosome-sized EVs (50–80 nm) including the score plot from the PCA (outliers removed) (A), PC-loading plot based on Raman shift (B), and average Raman spectra (C). PC-loading and spectrum intervals contributing to EV differences are highlighted.

the PBS. The largest PC-1 loadings, accounting for the strongest contributors to the differences found between $CD61^+$ and other EVs, could be seen at 984 and 1453 $cm^{-1}$, both accounted for proteins and lipids. The overlaid spectra in Fig. 3C additionally confirmed their major spectral differences. Moreover, according to the LDA result, 90% of the exomere-sized EVs were correctly classified. The findings demonstrated that exomere-sized $CD61^+$ EVs could be distinguished from other plasma-derived EVs sharing the same size, highlighting the possible differences in their overall biophysical compositions, cargoes, and functionalities.

Similar findings were obtained for exosome-sized EVs in which the $CD61^+$ EV cluster could be separated from $CD9^+$, $CD63^+$, and $CD81^+$ EV clusters (80% correctly classified according to LDA) in both PC-2 and PC-3 with several spectral ranges contributing to the variations (Fig. 4). The PC-2 loading highlighted their spectral differences at 1001 $cm^{-1}$ (protein: Phe), 1148-1245 $cm^{-1}$ (proteins and nucleic acids), 1310-1415 $cm^{-1}$ and 1551-1700 $cm^{-1}$ (proteins, lipids, and nucleic acids), and finally 1500-50 $cm^{-1}$ (proteins). On the other hand, PC-3 signified the differences contributing majorly from 892-1128 $cm^{-1}$ and 1280-1409 $cm^{-1}$ (proteins, lipids, and nucleic acids) and 900-1148 $cm^{-1}$ (proteins and lipids). The major peaks in both PCs contributing rather equally to the differences found at 830 $cm^{-1}$ (nucleic acids), 980 $cm^{-1}$ and 1030-33 $cm^{-1}$ (proteins and lipids), 1002 $cm^{-1}$ (proteins: Phe), 1239 $cm^{-1}$, and 1355 $cm^{-1}$ (nucleic acids and proteins). These

differences were also observed in the overlaid spectra (Fig. 4C).

In this study, $CD9^+$, $CD63^+$, and $CD81^+$ EVs represented subsets of plasma-derived EVs released from all possible cell origins into blood circulation that also contained the corresponding tetraspanin membrane proteins and were in the size ranges of exomeres and exosomes. These can include, but are not limited to, erythrocytes, leukocytes, and platelets [51,52]. On the other hand, $CD61^+$ or platelet-derived EVs were a subset of plasma-derived EVs specifically originating from platelets. Therefore, the differences in biochemical profiles between $CD61^+$ EVs and other EV subgroups could potentially result from different EV origins. For instance, we found that lipids contributed significantly to the differences in both EV sizes as also consistently reported by other studies involving discriminations of EVs from various cell types [7,53]. Since lipids are major membrane constituents of EVs and encapsulate bioactive compounds, the differences in lipids found in this study could imply that $CD61^+$ EVs differ from other EV subgroups in membrane compositions. Moreover, lipids in EVs have other several essential roles, such as being involved in EV biogenesis and intercellular communications [54]. The differences in proteins, also highly important molecules for cell-to-cell communication in EVs, further suggested that $CD61^+$ EVs might have distinct properties and biological roles. Along with lipids and proteins, we found that nucleic acids also contributed to the differences between the exosome-sized EVs. The heterogeneity of nucleic acid profiles between erythrocyte- and platelet-derived EVs have also been reported [55]. Altogether, the success in differentiating the platelet-derived EVs from other plasma-derived EVs for both exomere- and exosome-sized EVs confirmed the ability of Raman spectroscopy to distinguish EVs having different biological properties and origins even within the same size range.

*3.2.2.2. **$CD9^+$, $CD63^+$, $CD81^+$, and $CD61^+$ EV subpopulations.*** To take a more in-depth look into the influence of sizes on the differences in EV subpopulations, further PCAs were performed for $CD9^+$, $CD63^+$, $CD81^+$, and $CD61^+$ EV subpopulations categorized based on immunoaffinity ligands used during the isolation. The PC score plots resulting from spectra of $CD9^+$, $CD63^+$, $CD81^+$, and $CD61^+$ EVs (Fig. 5A, 5B, 5C, and 5D, respectively) indicated partial separation between the exomere- and exosome-sized EVs in which 75%, 65%, 60%, and 70% of the EVs were accurately classified based on the LDA results, respectively. The major differences between $CD9^+$ EVs of the two size ranges came mainly from 943-1030 $cm^{-1}$ (proteins and lipids) and slightly from 1304-1561 $cm^{-1}$ (proteins, lipids, and nucleic acids) (Fig. 5E). The most essential contributors to $CD9^+$ were the highest peaks at 980 $cm^{-1}$ (proteins and lipids) and 1450 $cm^{-1}$ (lipids) as also seen in the spectral differences in

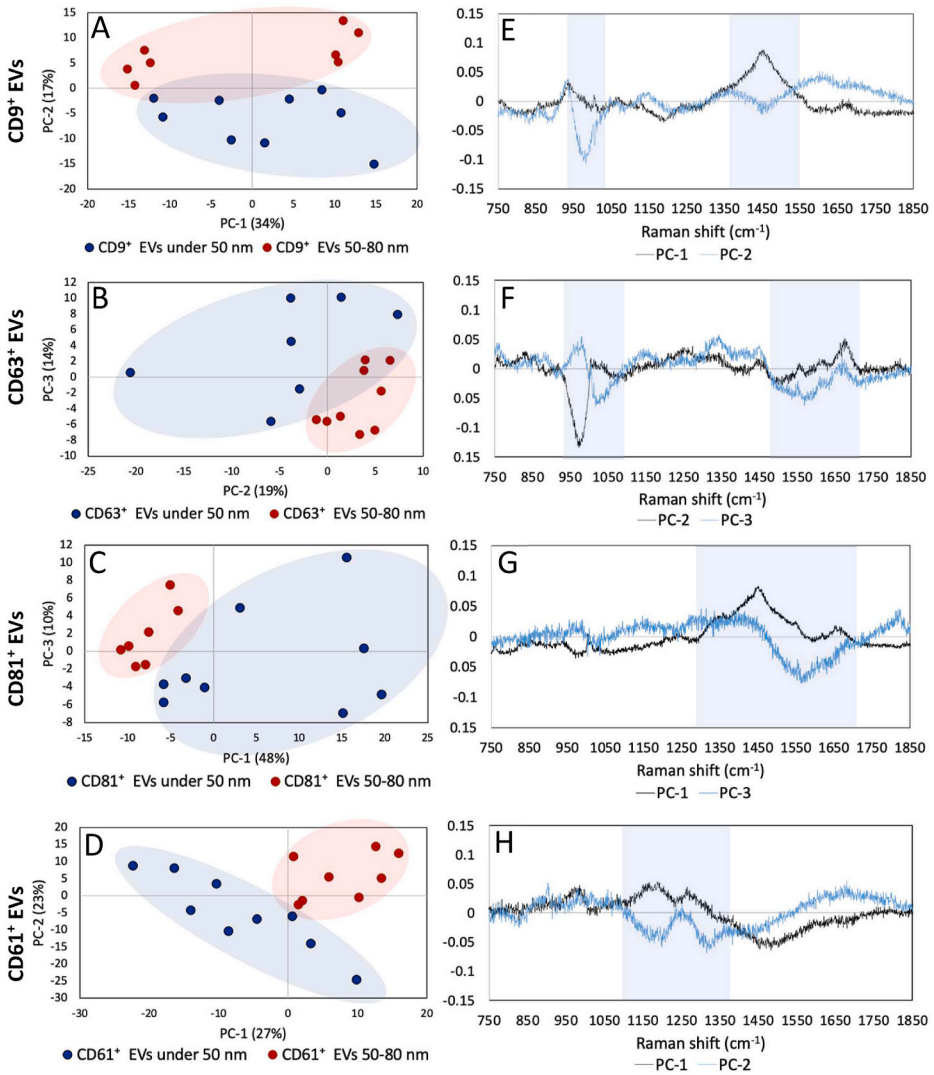


**Fig. 5.** Principal component analysis of EV subpopulations of their baseline-subtracted and SNV-normalized Raman spectra. Score plots of PCA from EV subpopulations based on immunoaffinity ligands used for the isolation (outliers removed): $CD9^+$ (A), $CD63^+$ (B), $CD81^+$ (C), and $CD61^+$ (D) EVs. Their PC loadings showing spectra contributing to differences in PCA are presented in (E), (F), (G), and (H), respectively.

Fig. S6. Similarly, proteins and lipids at 943-1030 $cm^{-1}$ also made the largest influence on the differences between $CD63^+$ EVs of two sizes, while proteins and other components made a minor contribution (1675 $cm^{-1}$ (proteins) and 1470-1645 $cm^{-1}$ (proteins, lipids, and nucleic acids)) (Fig. 5F). Interestingly, a slightly different trend was observed for $CD81^+$ EVs. Although the lipid and protein band at 943-1030 $cm^{-1}$ was also found to contribute to the variations between the two sizes of $CD81^+$ EVs, their main differences were caused by the spectral range of 1303–1577 $cm^{-1}$ in which 1460 $cm^{-1}$ (lipids) being the most dominant (Fig. 5G). In addition, PC-3 loading highlighted their small differences coming from proteins and lipids found at 1580 $cm^{-1}$. Opposite to other EV subpopulations, the differences between the two size ranges of $CD61^+$ EVs were mainly from proteins and nucleic acids at 1065-1260 $cm^{-1}$ and 1274-1377 $cm^{-1}$ as well as from the combination of proteins, nucleic acids, and lipids at 1353-1690 $cm^{-1}$ (Fig. 5H).

Overall, among exomere- and exosome-sized $CD9^+$, $CD63^+$, and $CD81^+$ EVs, lipids and proteins were the key contributors to the differences found in Raman spectra. Moreover, exomere- and exosome-sized $CD61^+$ EVs showed a similar trend, but proteins and nucleic acids contributed more strongly to the variations. The differences in lipids between the two EV sizes can be explained by the fact that the exosomes are membranous particles and thus are composed of lipid bilayer, while the recently discovered exomeres exhibit non-membranous characteristics as reported in the literature [3]. In addition, although biogenesis of exomeres is yet to be discovered, we can speculate that the differences in lipid and protein compositions between the exomere- and exosome-sized EVs can also be a result of different biogenesis processes. Consequently, EV subpopulations of both sizes can have distinct roles in physiology, supported by deviations in nucleic acid contents. In summary, Raman spectroscopy can rapidly and efficiently uncover the overall biochemical compositions of EV subpopulations and indicate the differences between EV origins. However, the technique only allows the general classification of the major groups of biological components, such as proteins and lipids, but not that of the specific constituents. The presence of two or more components can also result in overlapping frequency shifts, making it more challenging to determine the true and more specific contributors to the response especially in highly complex biological matrices, such as plasma-derived EVs. In order to further clarify, specify, and quantify the components that contributed to the differences found between EV subpopulations, additional chemical-specific investigations were needed.

### 3.3. Studies of the fatty acid composition of EV subpopulations by GCxGC—TOFMS

In this study, we have shown that Raman spectroscopy can reveal overall differences in biochemical compositions among the EV subpopulations. However, the technique only provided limited chemical-specific information on EV compositions. To get more in-depth information on EV lipids which were found to contribute to the differences among EVs by Raman spectroscopy, EV fatty acid compositions were studied using comprehensive GCxGC—TOFMS which has proven suitable for the separation of analytes having similar structures and properties, such as fatty acids, from highly complex matrices. Moreover, GCxGC—TOFMS also provides two and three-dimensional chromatograms, allowing for convenient visualization as well as identification and quantification of fatty acids. In general, fatty acids serve as building blocks of lipids in cell membranes and are involved in essential biological processes, including cell energy storage and transport, signaling, and mechanical protection [56,57], making them excellent candidates for further elucidation of EV structures and functions. Moreover, fatty acids are transported by the EVs and have been associated with biological processes, such as metabolism and tumor cell migration [58]. While it has been shown that exomere- and exosome-sized EVs have different cargoes and membrane structures, there is still very little known about the compositions of plasma-derived EVs, particularly exomeres. Analysis of fatty acids could also lead to clarification of their functions and signaling properties. For this purpose, we utilized high-resolution GCxGC—TOFMS for the identification and quantification of fatty acids present in the EV subpopulations as well as those in plasma and apoB-100-containing lipoproteins isolated before the characterization by the Raman spectroscopy by IAC-AsFlFFF. Details on fatty acids and chromatographic information used for their identification and quantification, including fatty acid classification, chromatograms, linearity, limits of detection, and quantification, can be found in Tables S1 and S3 and Fig. S7.

Fatty acids in plasma can generally be classified into two classes, namely esterified and non-esterified fatty acids [21] and can also be further divided into three subclasses based on their degree of unsaturation, including saturated (SAFA), monounsaturated (MUFA), and polyunsaturated (PUFA) fatty acids. In this study, esterified fatty acids represented fatty acids derived from the membrane structures of both lipoproteins and EVs, such as triglycerides and phospholipids, while non-esterified fatty acids came from free fatty acids stored inside the EVs or incorporated in their membrane structure. Fatty acids in all investigated samples were converted into FAMEs for GCxGC—TOFMS. In plasma, a total of 20 fatty acids were successfully identified and quantified (Fig. 6). Out of all detected fatty acids, C16:0, C16:1, C18:0, C18:1, C20:3, C20:4, and C22:6 fatty acids were present in relatively high amounts in the plasma esterified fatty acid fraction, supported by the literature [21]. The fatty acids enriched in plasma similarly existed in substantial amounts in the esterified fatty acid fraction of the apoB-100-containing lipoproteins, while only C16:0 and C18:0 fatty acids were abundant in the plasma non-esterified fatty acid fraction. Other fatty acids, except for the C18:0, were not detected in the non-esterified fatty acid fraction of apoB-100-containing lipoproteins, possibly due to the fact that lipids carried by VLDL and LDL are in esterified forms. These lipids include cholesterol esters and triglycerides, while their lipid membrane components are mainly phospholipids [29], resulting in a relatively high abundance of fatty acids found especially in the esterified fatty acid fraction.

Concerning the EV subpopulations, the fatty acids detected in their esterified fatty acid fractions were those commonly found in membrane lipids [54,59], including fatty acids with 16 and 18 carbon atoms in both saturated (C16:0 and C18:0) and unsaturated (including 16:1 and 18:1 in *cis* configuration) forms. The C16:0 fatty acid is the most common SAFA found in the human body and a major fatty acid found in glyco- and phospholipid membrane structures [60]. It has also been reported to be involved in several important functions in cells [61]. In addition to SAFAs, MUFAs, C18:1c fatty acids, were significantly enriched in the esterified fatty acid fractions of exomere-sized EVs and in the majority of the exosome-sized EVs. The detected C18:1c in this study could represent a mixture of oleic acid (C18:1n9c, the most common MUFA in membrane structure) and its positional isomers. It is well established that the oleic acid incorporated into cell membrane plays an important role as a regulator of membrane structure [62] (e.g., curvature), thus affecting biophysical characteristics and functions. Similarly, C16:1 found in membrane phospholipid structure [63] was present in a relatively low abundance in the esterified fatty acid fractions of most EVs. The presence of these fatty acids particularly in the esterified fatty acid fractions of the EV subpopulations can potentially be associated with their membrane properties, compositions, and synthesis.

In the non-esterified fatty acid (free fatty acids) fractions, C16:0 and C18:0 fatty acids were the most detected fatty acids in large amounts for the major EV subsets. The enrichment of these two fatty acids was in good agreement with an earlier study [64]. To our surprise, their abundance, especially in the exomere-sized EVs, was higher than their corresponding esterified fatty acid fractions in most cases. In addition to being one of the most common fatty acids in lipid membrane, the C16:0 fatty acid has been found to be associated with the induced release of hepatocyte-derived EVs and inflammatory responses in macrophages [65]. Moreover, the C18:0 fatty acid has been reported to take part as a

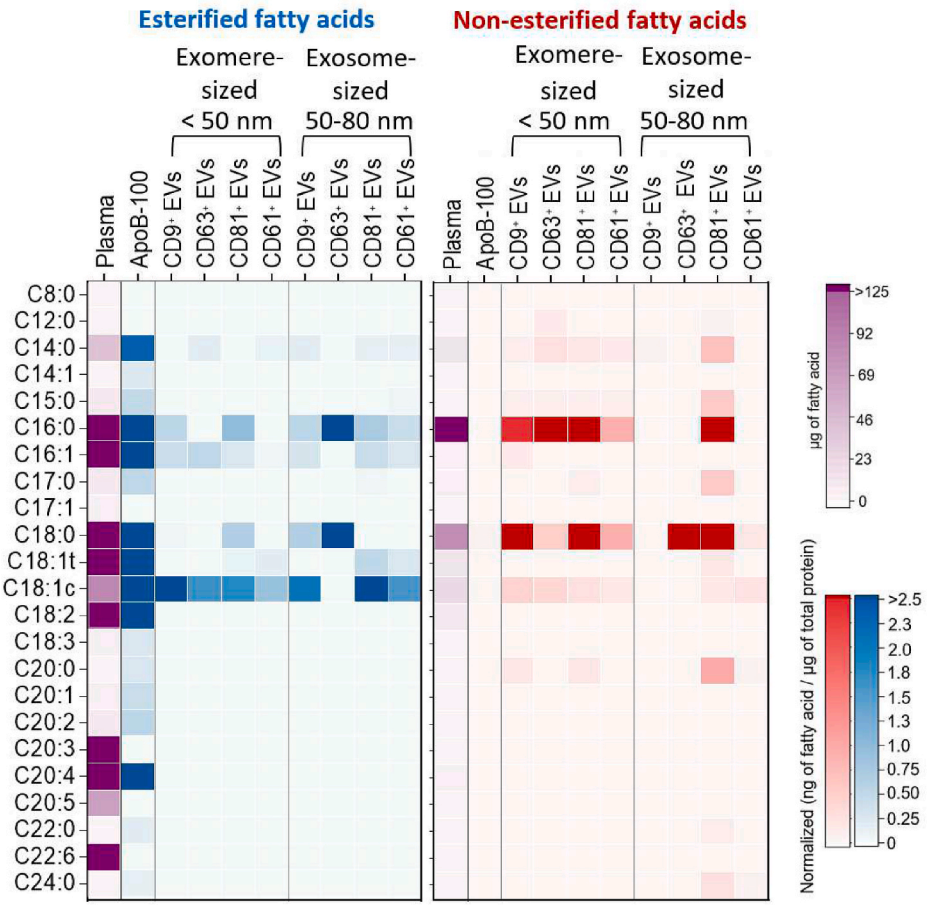


**Fig. 6.** Heat map visualization of esterified (left panel) and non-esterified fatty acids (right panel) in plasma (μg), apoB-100-containing-lipoproteins, and EV subpopulations (normalized with total protein contents: ng of fatty acid per μg of total protein) as measured by GCxGC—TOFMS. Information used for this heat map can be found in Tables S3 and S4.

signaling molecule in mitochondrial function regulation [66]. Although the underlying causes of this observation as well as functions of the free fatty acids carried by these EVs are yet to be elucidated, the findings as a whole suggest that these EVs could potentially participate in metabolism processes. Other SAFAs were also detected in the non-esterified fatty acid fractions of the EV subpopulations, including C14:0, C15:0, C20:0, C22:0, and C24:0. The last two, representing very long-chain fatty acids, were selectively enriched in exosome-sized CD61$^+$ and CD81$^+$ EVs, while these were absent in other EVs, suggesting that they might share some similar functionalities. Other studies have also reported that the free fatty acids enriched in exosomes were in saturated forms [64,67], which are consistent with our findings.

Overall, the results proved that most of the detected fatty acids in EVs are bioactive molecules that play important roles in the synthesis of the cell membrane, metabolism, and intercellular communication. The fatty acids detected in EVs corresponded to those present in plasma, and their abundance in EV subpopulations clearly differed (Fig. 6). The variations in membrane compositions could be seen from the different abundances in esterified fatty acid fractions. For instance, most fatty acids enriched in exomere-sized EVs in the esterified fatty acid fractions were found in lower amounts compared to their corresponding exosome-size EVs. These differences could result from various factors, such as size and nature of membrane characteristics (e.g., monolayer of exomere-sized EVs and bilayer of exosome-sized EVs). In comparison to other EV subpopulations, fatty acids in the non-esterified fatty acid fractions of the CD61$^+$ EVs (platelet-derived EVs) of both exomere- and exosome-sized were significantly lower, suggesting different cargoes. As it is known that EVs carry bioactive molecules that resemble their parental cells [68], this finding could imply that the origin of CD61$^+$ EVs was possibly different from other EVs as supported by the analysis of the Raman spectra where lipids were one of the key differences between CD61$^+$ and other EVs. The differences found among EV subpopulations even within the same size range underline the diversity of EVs in circulation, and further studies are required to fully elucidate their biological properties.

## 4. Conclusions

In this study, Raman spectroscopy was used to characterize CD9$^+$, CD63$^+$, CD81$^+$, and CD61$^+$ EV subpopulations of <50 nm exomere-sized and 50-80 exosome-sized, isolated and fractionated by our recently developed, novel IAC-AsFlFFF system. We found that by using Raman spectroscopy, EVs could be clearly distinguished from other plasma components, including apoB-100-containing lipoproteins, highlighting the application of Raman spectroscopy as a rapid and simple tool for quality control and EV purity assessment without the need for labeling. To obtain more chemical-specific information, GCxGC—TOFMS was thereafter used as a complementary technique to analyzed fatty acids in EVs and non-EV components. As a result, the differences between plasma, lipoproteins, and EV subpopulations were confirmed by their diverse fatty acid profiles. For both exomere- and exosome-sized EVs, Raman spectroscopy could further discriminate the platelet-derived (CD61$^+$) EVs from other EVs found in plasma, suggesting different compositions that could be due to different origins, with proteins and lipids being the two major contributors to the variations. Moreover, Raman spectroscopy allowed to distinguish size and

composition of exomere- and exosome-sized EVs isolated using the same immunoaffinity ligand, demonstrating Raman spectroscopy to be an excellent label-free technique of minimal sample preparation and volume. Raman spectroscopy settings used in this study were also simple and could provide a large amount of information in a short period of time (less than 30 s per sample). GCxGC—TOFMS further proved that EVs were composed of fatty acids necessary for various biological processes, including membrane construction, metabolism, and intercellular communications. The differences in fatty acid compositions of EV subpopulations supported the findings achieved by the Raman spectroscopic data that lipids contributed to the differences, not only between the platelet-derived EVs and other EVs but also between all analyzed EVs in this study, emphasizing the highly diverse nature of EVs found in the circulation. The applicability of Raman spectroscopy together with GCxGC—TOFMS can be extended to other EV applications that require elucidation and a better understanding of their biochemical composition and behavior, such as disease progression, diagnostic purposes, and further studies toward the understanding of the EV biogenesis, especially for exomere-sized EVs that are currently mostly unknown in terms of their biogenesis and functions.

## CRediT authorship contribution statement

**Thanaporn Liangsupree:** Investigation, Methodology, Formal analysis, Visualization, Writing – original draft. **Evgen Multia:** Investigation, Methodology, Reviewing and Editing. **Jukka Saarinen:** Instrumentation, Methodology, Reviewing and Editing. **Jose Ruiz-Jimenez:** Methodology, Formal analysis, Visualization, Reviewing and Editing. **Marianna Kemell:** Instrumentation, Methodology, Reviewing and Editing. **Marja-Liisa Riekkola:** Conceptualization, Supervision, Funding acquisition, Reviewing and Editing.

## Declaration of competing interest

The authors declare the following competing interest: Patent application (no. 20192643.3–1020).

## Acknowledgment

Financial support was provided by the Research Council for Natural Sciences and Engineering, Academy of Finland (grant number 1311369). Dr. Matti Jauhiainen and Minerva Foundation Insitute for Medical Research are thanked for providing the monoclonal anti-apoB-100 antibody and the facility for protein measurement. Dr. Katariina Öörni and Wihuri Research Institute are acknowledged for providing UC-isolated LDL. The use of ALD center Finland research infrastructure for FESEM imaging is acknowledged. Dr. Markus Metsälä, Assoc. Prof. Markku Vainio, and Severi Juttula are thanked for their help with the Raman spectrometer.

## Appendix A. Supplementary data

Supplementary data to this article can be found online at https://doi.org/10.1016/j.ab.2022.114672.

## References

[1] E.R. Abels, X.O. Breakefield, Introduction to extracellular vesicles: biogenesis, RNA cargo selection, content, release, and uptake, Cell. Mol. Neurobiol. 36 (2016) 301–312, https://doi.org/10.1007/s10571-016-0366-z.

[2] I.M. Chung, G. Rajakumar, B. Venkidasamy, U. Subramanian, M. Thiruvengadam, Exosomes: current use and future applications, Clin. Chim. Acta 500 (2020) 226–232, https://doi.org/10.1016/j.cca.2019.10.022.

[3] H. Zhang, D. Freitas, H.S. Kim, K. Fabijanic, Z. Li, H. Chen, M.T. Mark, H. Molina, A.B. Martin, L. Bojmar, J. Fang, S. Rampersaud, A. Hoshino, I. Matei, C.M. Kenific, M. Nakajima, A.P. Mutvei, P. Sansone, W. Buehring, H. Wang, J.P. Jimenez, L. Cohen-Gould, N. Paknejad, M. Brendel, K. Manova-Todorova, A. Magalhães, J. A. Ferreira, H. Osório, A.M. Silva, A. Massey, J.R. Cubillos-Ruiz, G. Galletti, P. Giannakakou, A.M. Cuervo, J. Blenis, R. Schwartz, M.S. Brady, H. Peinado, J. Bromberg, H. Matsui, C.A. Reis, D. Lyden, Identification of distinct nanoparticles and subsets of extracellular vesicles by asymmetric flow field-flow fractionation, Nat. Cell Biol. 20 (2018) 332–343, https://doi.org/10.1038/s41556-018-0040-4.

[4] E. Multia, C.J.Y. Tear, M. Palviainen, P. Siljander, M.L. Riekkola, Fast isolation of highly specific population of platelet-derived extracellular vesicles from blood plasma by affinity monolithic column, immobilized with anti-human CD61 antibody, Anal. Chim. Acta 1091 (2019) 160–168, https://doi.org/10.1016/j.aca.2019.09.022.

[5] E. Multia, T. Liangsupree, M. Jussila, J. Ruiz-Jimenez, M. Kemell, M.-L. Riekkola, Automated on-line isolation and fractionation system for nanosized biomacromolecules from human plasma, Anal. Chem. 9 (2020), https://doi.org/10.1021/acs.analchem.0c01986 acs.analchem.0c01986.

[6] T. Liangsupree, E. Multia, M.L. Riekkola, Modern isolation and separation techniques for extracellular vesicles, J. Chromatogr. A 1636 (2021) 461773, https://doi.org/10.1016/j.chroma.2020.461773.

[7] A. Gualerzi, S.A.A. Kooijmans, S. Niada, S. Picciolini, A.T. Brini, G. Camussi, M. Bedoni, Raman spectroscopy as a quick tool to assess purity of extracellular vesicle preparations and predict their functionality, J. Extracell. Vesicles 8 (2019) 1568780, https://doi.org/10.1080/20013078.2019.1568780.

[8] S.G. Kruglik, F. Royo, J.M. Guigner, L. Palomo, O. Seksek, P.Y. Turpin, I. Tatischeff, J.M. Falcón-Pérez, Raman tweezers microspectroscopy of: circa 100 nm extracellular vesicles, Nanoscale 11 (2019) 1661–1679, https://doi.org/10.1039/c8nr04677h.

[9] H. Zhang, A.C. Silva, W. Zhang, H. Rutigliano, A. Zhou, Raman Spectroscopy characterization extracellular vesicles from bovine placenta and peripheral blood mononuclear cells, PLoS One 15 (2020), e0235214, https://doi.org/10.1371/journal.pone.0235214.

[10] C.F. Morasso, D. Sproviero, M.C. Mimmi, M. Giannini, S. Gagliardi, R. Vanna, L. Diamanti, S. Bernuzzi, F. Piccotti, M. Truffi, O. Pansarasa, F. Corsi, C. Cereda, Raman spectroscopy reveals biochemical differences in plasma derived extracellular vesicles from sporadic Amyotrophic Lateral Sclerosis patients, Nanomed. Nanotechnol. Biol. Med. 29 (2020) 102249, https://doi.org/10.1016/j.nano.2020.102249.

[11] W. Lee, A. Nanou, L. Rikkert, F.A.W. Coumans, C. Otto, L.W.M.M. Terstappen, H. L. Offerhaus, Label-free prostate cancer detection by characterization of extracellular vesicles using Raman spectroscopy, Anal. Chem. 90 (2018) 11290–11296, https://doi.org/10.1021/acs.analchem.8b01831.

[12] T. Liangsupree, E. Multia, J. Metso, M. Jauhiainen, P. Forssén, T. Fornstedt, K. Öörni, A. Podgornik, M.-L. Riekkola, Rapid affinity chromatographic isolation method for LDL in human plasma by immobilized chondroitin-6-sulfate and anti-apoB-100 antibody monolithic disks in tandem, Sci. Rep. 9 (2019), https://doi.org/10.1038/s41598-019-47750-z.

[13] T. Liangsupree, E. Multia, P. Forssén, T. Fornstedt, M.-L. Riekkola, Kinetics and interaction studies of anti-tetraspanin antibodies and ICAM-1 with extracellular vesicle subpopulations using continuous flow quartz crystal microbalance biosensor, Biosens. Bioelectron. 206 (2022) 114151, https://doi.org/10.1016/J.BIOS.2022.114151.

[14] E. Multia, H. Sirén, K. Andersson, J. Samuelsson, P. Forssén, T. Fornstedt, K. Öörni, M. Jauhiainen, M.L. Riekkola, Thermodynamic and kinetic approaches for evaluation of monoclonal antibody - lipoprotein interactions, Anal. Biochem. 518 (2017) 25–34, https://doi.org/10.1016/j.ab.2016.10.024.

[15] P. Forssén, E. Multia, J. Samuelsson, M. Andersson, T. Aastrup, S. Altun, D. Wallinder, L. Wallbing, T. Liangsupree, M.L. Riekkola, T. Fornstedt, Reliable strategy for analysis of complex biosensor data, Anal. Chem. 90 (2018) 5366–5374, https://doi.org/10.1021/acs.analchem.8b00504.

[16] N. Gan, E. Multia, H. Sirén, M. Ruuth, K. Öörni, N.M. Maier, M. Jauhiainen, M. Kemell, M.L. Riekkola, Tailor-made approach for selective isolation and elution of low-density lipoproteins by immunoaffinity sorbent on silica, Anal. Biochem. 514 (2016) 12–23, https://doi.org/10.1016/j.ab.2016.09.005.

[17] P.K. Smith, R.I. Krohn, G.T. Hermanson, A.K. Mallia, F.H. Gartner, M. D. Provenzano, E.K. Fujimoto, N.M. Goeke, B.J. Olson, D.C. Klenk, Measurement of protein using bicinchoninic acid, Anal. Biochem. 150 (1985) 76–85, https://doi.org/10.1016/0003-2697(85)90442-7.

[18] R.J. Barnes, M.S. Dhanoa, S.J. Lister, Standard Normal Variate Transformation and De-trending of Near-Infrared Diffuse Reflectance Spectra vol. 43, 2016, pp. 772–777, https://doi.org/10.1366/0003702894202201.

[19] A. Bunn, M. Korpela, An Introduction to dplR, 2019, https://doi.org/10.1016/j.dendro.2008.01.002.

[20] W.S. Noble, What is a support vector machine? Nat. Biotechnol. (2006) 1565–1567, https://doi.org/10.1038/nbt1206-1565, 2006 2412. 24.

[21] N. Sánchez-Ávila, J.M. Mata-Granados, J. Ruiz-Jiménez, M.D. Luque de Castro, Fast, sensitive and highly discriminant gas chromatography-mass spectrometry method for profiling analysis of fatty acids in serum, J. Chromatogr. A 1216 (2009) 6864–6872, https://doi.org/10.1016/j.chroma.2009.08.045.

[22] S.T. Chin, Y. Bin Che Man, C.P. Tan, D.M. Hashim, Rapid profiling of animal-derived fatty acids using fast GC × GC coupled to Time-of-flight mass spectrometry, JAOCS, J. Am. Oil Chem. Soc. 86 (2009) 949–958, https://doi.org/10.1007/s11746-009-1427-y.

[23] M. Kopperi, J. Ruiz-Jiménez, J.I. Hukkinen, M.L. Riekkola, New way to quantify multiple steroidal compounds in wastewater by comprehensive two-dimensional gas chromatography-time-of-flight mass spectrometry, Anal. Chim. Acta 761 (2013) 217–226, https://doi.org/10.1016/j.aca.2012.11.059.

[24] M.-P. Caby, D. Lankar, C. Vincendeau-Scherrer, G. Raposo, C. Bonnerot, Exosomal-like vesicles are present in human blood plasma, Int. Immunol. 17 (2005) 879–887, https://doi.org/10.1093/intimm/dxh267.

[25] I. Barranco, L. Padilla, I. Parrilla, A. Álvarez-Barrientos, C. Pérez-Patiño, F.J. Peña, E.A. Martínez, H. Rodriguez-Martínez, J. Roca, Extracellular vesicles isolated from porcine seminal plasma exhibit different tetraspanin expression profiles, Sci. Rep. 9 (2019), https://doi.org/10.1038/s41598-019-48095-3.

[26] S.S. Lee, J.H. Won, G.J. Lim, J. Han, J.Y. Lee, K.O. Cho, Y.K. Bae, A novel population of extracellular vesicles smaller than exosomes promotes cell proliferation, Cell Commun. Signal. 17 (2019) 95, https://doi.org/10.1186/s12964-019-0401-z.

[27] E. Willms, C. Cabañas, I. Mäger, M.J.A. Wood, P. Vader, Extracellular vesicle heterogeneity: subpopulations, isolation techniques, and diverse functions in cancer progression, Front. Immunol. 9 (2018) 1, https://doi.org/10.3389/fimmu.2018.00738.

[28] J.B. German, J.T. Smilowitz, A.M. Zivkovic, Lipoproteins: when size really matters, Curr. Opin. Colloid Interface Sci. 11 (2006) 171–183, https://doi.org/10.1016/j.cocis.2005.11.006.

[29] D.A. Bricarello, J.T. Smilowitz, A.M. Zivkovic, J.B. German, A.N. Parikh, Reconstituted lipoprotein: a versatile class of biologically-inspired nanostructures, ACS Nano 5 (2011) 42–57, https://doi.org/10.1021/nn103098m.

[30] H.M. Colhoun, J.D. Otvos, M.B. Rubens, M.R. Taskinen, S. Richard Underwood, J. H. Fuller, Lipoprotein subclasses and particle sizes and their relationship with coronary artery calcification in men and women with and without type 1 diabetes, Diabetes 51 (2002) 1949–1956, https://doi.org/10.2337/diabetes.51.6.1949.

[31] J.E. Romanchik, E.H. Harrison, D.W. Morel, Addition of lutein, lycopene, or β-carotene to LDL or serum in vitro: effects on carotenoid distribution, LDL composition, and LDL oxidation, J. Nutr. Biochem. 8 (1997) 681–688, https://doi.org/10.1016/S0955-2863(97)00119-8.

[32] Z. Movasaghi, S. Rehman, I.U. Rehman, Raman spectroscopy of biological tissues, Appl. Spectrosc. Rev. 42 (2007) 493–541, https://doi.org/10.1080/05704920701551530.

[33] Z. Huang, A. McWilliams, H. Lui, D.I. McLean, S. Lam, H. Zeng, Near-infrared Raman spectroscopy for optical diagnosis of lung cancer, Int. J. Cancer 107 (2003) 1047–1052, https://doi.org/10.1002/ijc.11500.

[34] G. Shetty, C. Kendall, N. Shepherd, N. Stone, H. Barr, Raman spectroscopy: elucidation of biochemical changes in carcinogenesis of oesophagus, Br. J. Cancer 94 (2006) 1460–1464, https://doi.org/10.1038/sj.bjc.6603102.

[35] A.J. Ruiz-Chica, M.A. Medina, F. Sánchez-Jiménez, F.J. Ramírez, Characterization by Raman spectroscopy of conformational changes on guanine-cytosine and adenine-thymine oligonucleotides induced by aminooxy analogues of spermidine, J. Raman Spectrosc. 35 (2004) 93–100, https://doi.org/10.1002/jrs.1107.

[36] R. Jyothi, M. Krishna, R. Solomon, Tissue Raman spectroscopy for the study of radiation damage: Brain irradiation of mice. Https://Doi.Org/10.1667/0033-7587(2002)157[0175:TRSFTS]2.0.CO;2, 2002, 157, https://doi.org/10.1667/0033, 175-182.

[37] D.P. Lau, Z. Huang, H. Lui, C.S. Man, K. Berean, M.D. Morrison, H. Zeng, Raman spectroscopy for optical diagnosis in normal and cancerous tissue of the nasopharynx - preliminary findings, Laser Surg. Med. 32 (2003) 210–214, https://doi.org/10.1002/lsm.10084.

[38] S. Koljenović, T.B. Schut, A. Vincent, J.M. Kros, G.J. Puppels, Detection of meningioma in dura mater by Raman spectroscopy, Anal. Chem. 77 (2005) 7958–7965, https://doi.org/10.1021/ac0512599.

[39] N.J. Kline, P.J. Treado, Raman chemical imaging of breast tissue, J. Raman Spectrosc. 28 (1997) 119–124, https://doi.org/10.1002/(sici)1097-4555(199702)28:2/3<119::aid-jrs73>3.0.co;2-3.

[40] H. Schulz, M. Baranska, Identification and quantification of valuable plant substances by IR and Raman spectroscopy, Vib. Spectrosc. 43 (2007) 13–25, https://doi.org/10.1016/j.vibspec.2006.06.001.

[41] Y.D. Winters, T.K. Lowenstein, M.N. Timofeeff, Identification of carotenoids in ancient salt from death valley, saline valley, and searles lake, California, using laser Raman spectroscopy, Astrobiology 13 (2013) 1065–1080, https://doi.org/10.1089/ast.2012.0952.

[42] N. Stone, C. Kendall, J. Smith, P. Crow, H. Barr, Raman spectroscopy for identification of epithelial cancers, Faraday Discuss 126 (2004) 141–157, https://doi.org/10.1039/b304992b.

[43] W.-T. Cheng, M.-T. Liu, H.-N. Liu, S.-Y. Lin, Micro-Raman spectroscopy used to identify and grade human skin pilomatrixoma, Microsc. Res. Tech. 68 (2005) 75–79, https://doi.org/10.1002/jemt.20229.

[44] C. Krafft, L. Neudert, T. Simat, R. Salzer, Near infrared Raman spectra of human brain lipids, Spectrochim. Acta Part A Mol. Biomol. Spectrosc. 61 (2005) 1529–1535, https://doi.org/10.1016/j.saa.2004.11.017.

[45] J.W. Chan, D.S. Taylor, T. Zwerdling, S.M. Lane, K. Ihara, T. Huser, Micro-Raman spectroscopy detects individual neoplastic and normal hematopoietic cells, Biophys. J. 90 (2006) 648–656, https://doi.org/10.1529/biophysj.105.066761.

[46] I. Notingher, C. Green, C. Dyer, E. Perkins, N. Hopkins, C. Lindsay, L.L. Hench, Discrimination between ricin and sulphur mustard toxicity in vitro using Raman spectroscopy, J. R. Soc. Interface 1 (2004) 79–90, https://doi.org/10.1098/rsif.2004.0008.

[47] R. Malini, K. Venkatakrishna, J. Kurien, K.M. Pai, L. Rao, V.B. Kartha, C. M. Krishna, Discrimination of normal, inflammatory, premalignant, and malignant oral tissue: a Raman spectroscopy study, Biopolymers 81 (2006) 179–193, https://doi.org/10.1002/bip.20398.

[48] E. Ó Faoláin, M.B. Hunter, J.M. Byrne, P. Kelehan, M. McNamara, H.J. Byrne, F. M. Lyng, A study examining the effects of tissue processing on human tissue sections using vibrational spectroscopy, in: Vib. Spectrosc, Elsevier, 2005, pp. 121–127, https://doi.org/10.1016/j.vibspec.2005.02.013.

[49] E.B. Hanlon, R. Manoharan, T.W. Koo, K.E. Shafer, J.T. Motz, M. Fitzmaurice, J. R. Kramer, I. Itzkan, R.R. Dasari, M.S. Feld, Prospects for in vivo Raman spectroscopy, Phys. Med. Biol. 45 (2000) R1, https://doi.org/10.1088/0031-9155/45/2/201.

[50] M.D. Fontana, K. Ben Mabrouk, T.H. Kauffmann, Raman spectroscopic sensors for inorganic salts, Spectrosc. Prop. Inorg. Organomet. C 44 (2013) 40–67, https://doi.org/10.1039/9781849737791-00040.

[51] K. Thangaraju, S.N. Neerukonda, U. Katneni, P.W. Buehler, Extracellular vesicles from red blood cells and their evolving roles in health, coagulopathy and therapy, Int. J. Mol. Sci. 22 (2021) 1–25, https://doi.org/10.3390/ijms22010153.

[52] L.H. Pugholm, R. Bæk, E.K.L. Søndergaard, A.L.S. Revenfeld, M.M. Jørgensen, K. Varming, Phenotyping of leukocytes and leukocyte-derived extracellular vesicles, J. Immunol. Res. 2016 (2016), https://doi.org/10.1155/2016/6391264.

[53] Z.J. Smith, C. Lee, T. Rojalin, R.P. Carney, S. Hazari, A. Knudson, K. Lam, H. Saari, E.L. Ibañez, T. Viitala, T. Laaksonen, M. Yliperttula, S. Wachsmann-Hogiu, Single exosome study reveals subpopulations distributed among cell lines with variability related to membrane content, J. Extracell. Vesicles 4 (2015), https://doi.org/10.3402/jev.v4.28533.

[54] T. Skotland, K. Sagini, K. Sandvig, A. Llorente, An emerging focus on lipids in extracellular vesicles, Adv. Drug Deliv. Rev. 159 (2020) 308–321, https://doi.org/10.1016/j.addr.2020.03.002.

[55] K. Kondratov, Y. Nikitin, A. Fedorov, A. Kostareva, V. Mikhailovskii, D. Isakov, A. Ivanov, A. Golovkin, Heterogeneity of the nucleic acid repertoire of plasma extracellular vesicles demonstrated using high-sensitivity fluorescence-activated sorting, J. Extracell. Vesicles 9 (2020) 1743139, https://doi.org/10.1080/20013078.2020.1743139.

[56] C.C.C.R. De Carvalho, M.J. Caramujo, The various roles of fatty acids, Molecules 23 (2018), https://doi.org/10.3390/molecules23102583.

[57] E. Tvrzická, M. Vecka, B. Staňková, A. Žák, Analysis of fatty acids in plasma lipoproteins by gas chromatography-flame ionization detection: quantitative aspects, Anal. Chim. Acta 465 (2002) 337–350, https://doi.org/10.1016/S0003-2670(02)00396-3.

[58] E. Clement, I. Lazar, C. Attané, L. Carrié, S. Dauvillier, M. Ducoux-Petit, D. Esteve, T. Menneteau, M. Moutahir, S. Le Gonidec, S. Dalle, P. Valet, O. Burlet-Schiltz, C. Muller, L. Nieto, Adipocyte extracellular vesicles carry enzymes and fatty acids that stimulate mitochondrial metabolism and remodeling in tumor cells, EMBO J. 39 (2020), e102525, https://doi.org/10.15252/embj.2019102525.

[59] V.S. Shramko, Y.V. Polonskaya, E.V. Kashtanova, E.M. Stakhneva, Y.I. Ragino, The short overview on the relevance of fatty acids for human cardiovascular disorders, Biomolecules 10 (2020) 1–24, https://doi.org/10.3390/biom10081127.

[60] G. Carta, E. Murru, S. Banni, C. Manca, Palmitic acid: physiological role, metabolism and nutritional implications, Front. Physiol. 8 (2017) 902, https://doi.org/10.3389/fphys.2017.00902.

[61] J. Korbecki, K. Bajdak-Rusinek, The effect of palmitic acid on inflammatory response in macrophages: an overview of molecular mechanisms, Inflamm. Res. 68 (2019) 915–932, https://doi.org/10.1007/s00011-019-01273-5.

[62] S. Lopez, B. Bermudez, S. Montserrat-De La Paz, S. Jaramillo, L.M. Varela, A. Ortega-Gomez, R. Abia, F.J.G. Muriana, Membrane composition and dynamics: a target of bioactive virgin olive oil constituents, Biochim. Biophys. Acta Biomembr. 1838 (2014) 1638–1656, https://doi.org/10.1016/j.bbamem.2014.01.007.

[63] C. Ferreri, A. Masi, A. Sansone, G. Giacometti, A. Larocca, G. Menounou, R. Scanferlato, S. Tortorella, D. Rota, M. Conti, S. Deplano, M. Louka, A. Maranini, A. Salati, V. Sunda, C. Chatgilialoglu, Fatty acids in membranes as homeostatic, metabolic and nutritional biomarkers: recent advancements in analytics and diagnostics, Diagnostics 7 (2016) 1, https://doi.org/10.3390/diagnostics7010001.

[64] C. Subra, D. Grand, K. Laulagnier, A. Stella, G. Lambeau, M. Paillasse, P. De Medina, B. Monsarrat, B. Perret, S. Silvente-Poirot, M. Poirot, M. Record, Exosomes account for vesicle-mediated transcellular transport of activatable phospholipases and prostaglandins, J. Lipid Res. 51 (2010) 2105–2120, https://doi.org/10.1194/jlr.M003657.

[65] P. Hirsova, S.H. Ibrahim, A. Krishnan, V.K. Verma, S.F. Bronk, N.W. Werneburg, M. R. Charlton, V.H. Shah, H. Malhi, G.J. Gores, Lipid-induced signaling causes release of inflammatory extracellular vesicles from hepatocytes, Gastroenterology 150 (2016) 956–967, https://doi.org/10.1053/j.gastro.2015.12.037.

[66] D. Senyilmaz-Tiebe, D.H. Pfaff, S. Virtue, K.V. Schwarz, T. Fleming, S. Altamura, M.U. Muckenthaler, J.G. Okun, A. Vidal-Puig, P. Nawroth, A.A. Teleman, Dietary stearic acid regulates mitochondria in vivo in humans, Nat. Commun. 9 (2018) 1–10, https://doi.org/10.1038/s41467-018-05614-6.

[67] R.A. Haraszti, M.C. Didiot, E. Sapp, J. Leszyk, S.A. Shaffer, H.E. Rockwell, F. Gao, N.R. Narain, M. DiFiglia, M.A. Kiebish, N. Aronin, A. Khvorova, High-resolution proteomic and lipidomic analysis of exosomes and microvesicles from different cell sources, J. Extracell. Vesicles 5 (2016), https://doi.org/10.3402/jev.v5.32570.

[68] N. Ludwig, T.L. Whiteside, T.E. Reichert, Challenges in exosome isolation and analysis in health and disease, Int. J. Mol. Sci. 20 (2019), https://doi.org/10.3390/ijms20194684.